nature nanotechnology

LETTERS

PUBLISHED ONLINE: 13 MAY 2012 | DOI: 10.1038/NNANO.2012.69

Virus-based piezoelectric energy generation

Byung Yang Lee[1,4], Jinxing Zhang[2,5], Chris Zueger[3,4], Woo-Jae Chung[1,4], So Young Yoo[1,4], Eddie Wang[1,4], Joel Meyer[1,4], Ramamoorthy Ramesh[2,5] and Seung-Wuk Lee[1,4]*

Piezoelectric materials can convert mechanical energy into electrical energy[1,2], and piezoelectric devices made of a variety of inorganic materials[3–5] and organic polymers[6] have been demonstrated. However, synthesizing such materials often requires toxic starting compounds, harsh conditions and/or complex procedures[7]. Previously, it was shown that hierarchically organized natural materials such as bones[8], collagen fibrils[9,10] and peptide nanotubes[11,12] can display piezoelectric properties. Here, we demonstrate that the piezoelectric and liquid-crystalline properties of M13 bacteriophage (phage) can be used to generate electrical energy. Using piezoresponse force microscopy, we characterize the structure-dependent piezoelectric properties of the phage at the molecular level. We then show that self-assembled thin films of phage can exhibit piezoelectric strengths of up to 7.8 pm V^{-1}. We also demonstrate that it is possible to modulate the dipole strength of the phage, hence tuning the piezoelectric response, by genetically engineering the major coat proteins of the phage. Finally, we develop a phage-based piezoelectric generator that produces up to 6 nA of current and 400 mV of potential and use it to operate a liquid-crystal display. Because biotechnology techniques enable large-scale production of genetically modified phages, phage-based piezoelectric materials potentially offer a simple and environmentally friendly approach to piezoelectric energy generation.

Owing to their well-defined shape and ability to display functional peptides through genetic and chemical modification, M13 phage and other viral particles have already been used to fabricate functional materials for inorganic nanomaterial synthesis and assembly[13–15], energy storage and generation[16,17] and tissue regeneration[18,19]. Phage can be produced simply and economically by infecting bacteria. The phage then co-opts the bacterial metabolism to continuously synthesize and secrete new phage particles, leading to millions of copies after culturing overnight (for details see Supplementary Information). Structurally, M13 phage has a long rod-like shape, ~880 nm in length and 6.6 nm in diameter (Fig. 1a)[20,21]. Each phage is covered by ~2,700 copies of a major coat protein (pVIII) and five copies of minor coat proteins (pIII and pIX) located at either end. The pVIII proteins have an α-helical structure with a dipole moment directed from the amino- to the carboxy-terminal direction and cover the body of the phage with five-fold rotational and two-fold screw symmetry (Fig. 1b–d). Because the M13 aligned protein coat structure lacks inversion symmetry, we expected the phage to demonstrate intrinsic piezoelectric properties.

We first characterized the piezoelectric properties of the phage at a molecular level. To do so, we made use of piezoresponse force microscopy (PFM), in which the mechanical response of the material was monitored while applying an electrical signal through a metal-coated atomic force microscope (AFM) tip and scanning the sample (Fig. 2a, Supplementary Movie S1)[22]. To characterize the structure-dependent piezoelectric properties at the single-phage level, we fabricated self-assembled phage monolayer films, patterned as 1-μm-wide lines, on gold substrates (for detailed method see Supplementary Information)[23]. AFM topography analysis (Fig. 2b) showed ~7-nm-high phage monolayers with a directionally ordered nematic structure. Piezoresponse force microscopy characterization revealed that the piezoelectric phage responded to an applied electric field in both lateral and axial directions (Fig. 2c–e). For lateral PFM, when scanning along the long axes of the phage (Fig. 2c), the films exhibited characteristic bright and dark fibril textures. When we performed lateral PFM perpendicular to the long axes by rotating the sample through 90°, the fibril texture contrast disappeared (Fig. 2d). The contrast in Fig. 2c is probably a result of the net dipole moment of the phage along its axial direction, which causes the cantilever to undergo torsion in opposite directions when probing phages that are oriented antiparallel to one another (Fig. 2f). However, in the case of Fig. 2d, the tilt angle (~20°) of the α-helical coat proteins with respect to the phage axis[24] (Fig. 1d) and the helical screw advancement of the dipole[25] result in a radial component that is independent of orientation (Fig. 2f). These responses show the existence of shear piezoelectricity. Meanwhile, the axial response (Fig. 2e) shows the existence of compressive piezoelectricity, presumably due to the breaking of the fivefold rotational symmetry under an electric field.

Having verified the inherent piezoelectric response of the phage fibres, we modulated the piezoelectric strength of the phage by engineering the pVIII coat protein using recombinant DNA techniques. Because the pVIII coat protein dipole should be induced mainly by its charge distribution (that is, the densely packed positive charges near the C-terminus and the densely packed negative charges near the N-terminus; Fig. 2g), we engineered the pVIII N-terminus with a variable number of the negatively charged amino-acid glutamate (E). The residues (from one (1E) to four (4E)) were inserted between the first (Ala) and fifth (Asp) amino acids of the wild-type pVIII major coat sequence (Fig. 1e). The wild-type sequence contains two negative charges within the insert region, so 4E-phage displays two additional negative charges and 1E-phage displays one less negative charge than the wild-type phage (protein sequences are available in the Supplementary Information). Phage monolayers were prepared with 1E-, 2E-, 3E- and 4E-phages as described previously[26]. These genetically engineered phages exhibited a chemical structure-dependent piezoelectric response (Fig. 2h). Vertical PFM measurements revealed that the effective piezoelectric coefficient (d_{eff}) of the wild-type phage, calculated from the slope of the PFM amplitude versus the applied voltage curve, was 0.30 ± 0.03 pm V^{-1}. We observed that

[1]Department of Bioengineering, University of California, Berkeley, California 94720, USA, [2]Department of Materials Science and Engineering, University of California, Berkeley, California 94720, USA, [3]Department of Mechanical Engineering, University of California, Berkeley, California 94720, USA, [4]Physical Biosciences Division, Lawrence Berkeley National Laboratory, Berkeley, California 94720, USA, [5]Materials Science Division, Lawrence Berkeley National Laboratory, Berkeley, California 94720, USA. *e-mail: leesw@berkeley.edu

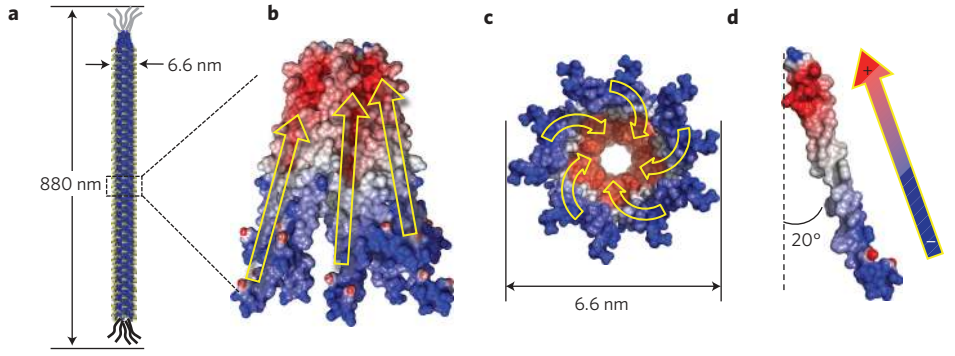

Figure 1 | Schematic of piezoelectric M13 phage structure. a, The M13 phage is ~880 nm in length and ~6.6 nm in diameter, is covered by ~2,700 pVIII coat proteins and has five copies each of pIII (grey lines) and pIX (black lines) proteins at either end. **b**, Side view of the electrostatic potential of M13 phage after bioengineered modification with four glutamate amino acids. The dipole moments generated by ten α-helical major coat proteins are directed from the N-terminus (blue) to the C-terminus (red). Yellow arrows indicate dipole direction. **c**, Vertical cross-sectional view of the electrostatic potential of M13 phage. The pVIII coat proteins assemble with five-fold rotational and two-fold screw symmetry. **d**, Side-view representation of the electrostatic potential of a single M13-phage pVIII coat protein. The pVIII coat protein has an ~20° tilt angle with respect to the phage long axis. The colours of the molecular surface indicate positive (red), neutral (white) and negative (blue) electrostatic potentials. Yellow arrows filled with two colours (red and blue) represent the dipole pointing from negative (blue) to positive (red) regions. **e**, Primary structure of the engineered major coat protein. Amino acids with positively and negatively charged side chains are labelled in red and blue, respectively. The engineered four-glutamate (4E) amino-acid sequence is underlined.

the 1E-phage had the lowest d_{eff} value of 0.14 ± 0.03 pm V^{-1}, with an increase in d_{eff} for each additional negative charge up to the 4E-phage, which exhibited the highest value of 0.70 ± 0.05 pm V^{-1}. The wild-type phage exhibited a response similar to that of the 2E-phage, as expected because of their similar charge distributions.

The piezoelectric properties of the phage could be further enhanced by controlling the thickness of the phage films as verified by preparing multilayer phage films of varying thicknesses using the 4E-phage (for detailed methods see Supplementary Information). An AFM topography image (Fig. 3a) of a phage film shows that it has a smectic structure (ordered in both direction and position) with a band spacing of ~1 μm (Fig. 3a and inset). The phage particles formed a ridge and groove band pattern, composed of the pVIII major coat proteins, and the pIII and pIX minor coat proteins, respectively (Fig. 3b). We measured the mechanical properties of our multilayer phage films using nanoindentation (for details see Supplementary Information). The films had a hardness of $H = 214.0 \pm 21.4$ MPa and Young's modulus of $E = 4.1 \pm 0.6$ GPa (Supplementary Fig. S1). A piezoelectric coefficient mapping image showed that d_{eff} of the ridge areas was higher than that of the groove areas. Additionally, the observed piezoelectric response was dependent on the film thickness (Fig. 3c). The phage films exhibited an increased effective piezoelectric coefficient with increasing film thickness up to a saturated level of $d_{eff} \approx 3.9$ pm V^{-1} for films greater than ~100 nm thick. The increased piezoresponse with film thickness is presumably due to a corresponding decrease in the contribution from the substrate clamping effect[27]. Because a non-uniform electric field was applied to the sample through the AFM tip during the piezoelectric measurements, the relationship between d_{eff}, obtained from the PFM measurements, and the piezoelectric coefficient d_{33} is not straightforward[28]. Previously, it has been reported that, in the weak indentation regime, where the indentation of the AFM tip into the sample (~2 nm) is less than the tip radius (~10 nm), the d_{33} value can be approximated by $d_{eff} = 0.5 \times d_{33}$ (ref. 22). Based on this relationship, we can estimate the actual d_{33} value of the phage film to be 7.8 pm V^{-1}.

Using the same piezoelectric measurement set-up, we compared the piezoelectric response of the phage film with two control piezoelectric materials, periodically poled lithium niobate (PPLN) and type I collagen films (Supplementary Fig. S2; for details see Supplementary Information). The d_{33} values of PPLN and collagen were 13.2 and 1.1 pm V^{-1}, respectively (Fig. 3d), which are similar to previously reported values[29]. It should be noted that the rather low d_{33} value for collagen arises because collagen displays a piezoelectric response mainly in the axial direction, rather than radially[30].

Finally, we investigated whether humidity would alter the piezoresponse, because water content is known to affect the piezoelectricity of other organic materials[31]. The phage film showed similar piezoresponses within the relative humidity range 30–70%, but these decreased to ~1.5 pm V^{-1} at a relative humidity >80% (Supplementary Fig. S3).

Using 4E-phage films, we fabricated phage-based piezoelectric energy generators. First, spontaneously ordered multilayer phage films with an area of ~1 cm^2 were created between two gold electrodes by dropcasting (Fig. 4a; for detailed methods see Supplementary Information). Periodic mechanical loads were applied to the phage-based piezoelectric generators using a dynamic mechanical test system, and the resultant electrical output signal was characterized by measuring the short-circuit current, open-circuit voltage and charge (Fig. 4b). When applying a rectangular compressive load (Fig. 4c) at 6 s intervals, the signal showed two peaks of reverse polarity, which correspond to the pressing and releasing motion of the mechanical test system. From this experiment, we typically observed peak values of ~4 nA for the short-circuit current (Fig. 4d). The integral of a single peak gives the charge value, $Q \approx 380$ pC, generated at applied peak load of $F = 34$ N. Using the equation for a quasi-static piezoelectric coefficient $d_{33} = Q/F$ (ref. 32), we can roughly estimate the piezoelectric coefficient as $d_{33} = 11.2 \pm 0.7$ pm V^{-1}, which is similar to the value measured by PFM. The open-circuit voltage shows a peak voltage value of 400 mV and a decay time constant of ~0.3 s (Fig. 4e). A connection polarity reversion test showed that the current and voltage signals were reversed when the device polarity was switched, indicating that the electrical signals came from the phage material and not from electrostatic interactions (Supplementary Fig. S4). We confirmed that the piezoelectric energy generation originated only from the phage films by using a charge amplifier, which exhibited

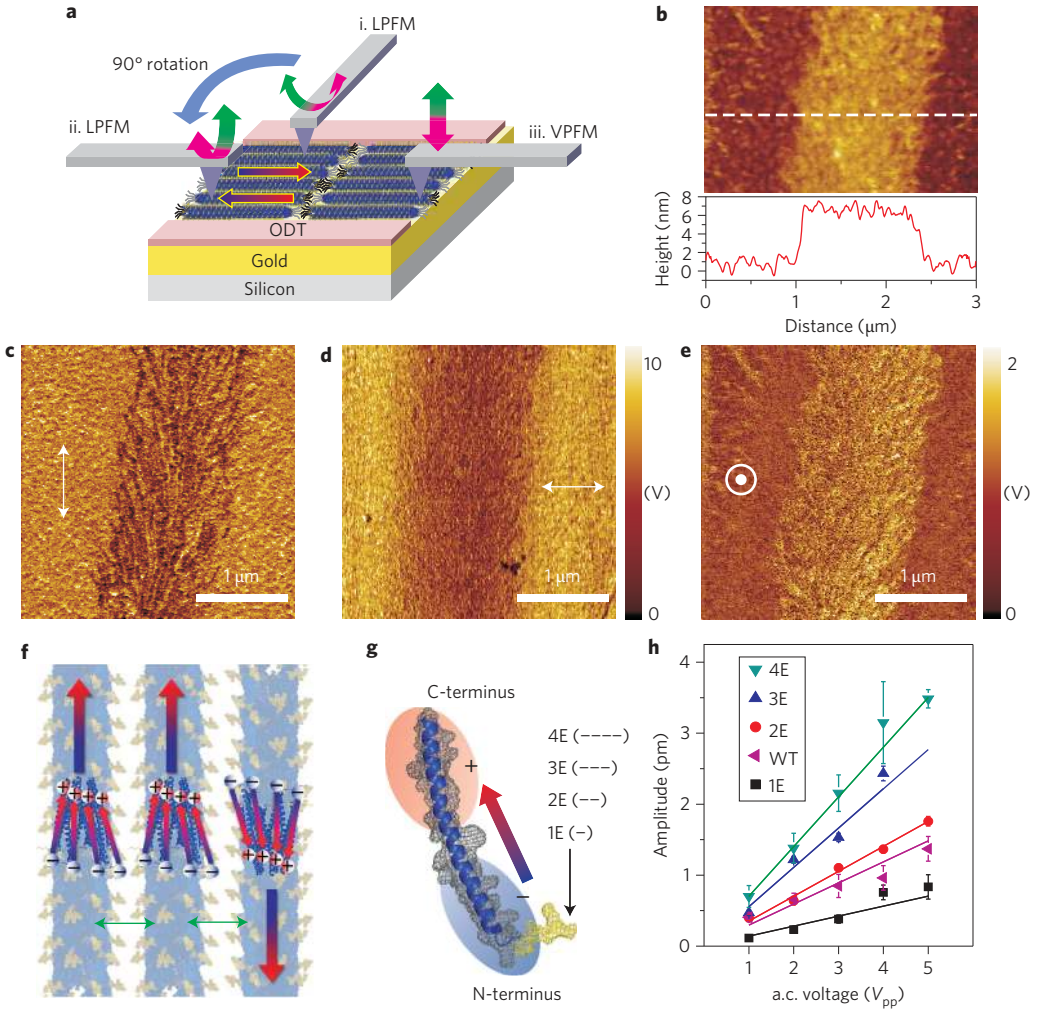

Figure 2 | Piezoelectric properties of monolayer phage films. a, Schematic of the PFM measurement. A single layer of phages was assembled on a molecularly patterned gold substrate and PFM responses were measured using lateral PFM (LPFM; i and ii) and vertical PFM (VPFM, iii) modes. **b**, AFM topography (top) and height profile (bottom) of a monolayer phage film. **c**, Lateral PFM image of the monolayer phage film. The lateral PFM signal originates from the torsional motion of the AFM tip along the phage long axis direction (depicted in **a**(i)). **d**, Lateral PFM image obtained after changing the scanning direction by 90° (depicted in **a**(ii)). The colour scale applies to both **c** and **d. e**, Vertical PFM image of the monolayer phage film (depicted in **a**(iii)). The vertical PFM signal is collected from the vertical motion of the AFM tip. **f**, Schematic depicting phage with randomly mixed dipoles through the axial direction of the monolayer, which exhibit both axial (red–blue arrows) and radial (green arrows) components of the dipole moments. **g**, Schematic of a single pVIII protein with dipole strength that is tunable by modulating the number of glutamates (E; yellow) at its N-terminus. **h**, Comparison of out-of-plane PFM amplitudes versus applied a.c. peak-to-peak voltage (V_{pp}) between phages with genetically engineered coat proteins. Error bars indicate one standard deviation. 1E-, wild-type (WT)-, 2E-, 3E- and 4E-phage monolayer films exhibited effective piezoelectric coefficient d_{eff} values of 0.14 ± 0.03, 0.30 ± 0.03, 0.35 ± 0.01, 0.55 ± 0.03 and 0.70 ± 0.05 pm V^{-1}, respectively.

a similar charge output signal and reversible polarity (Supplementary Figs S5–S7). We also investigated the effects of strain amplitude and rate on the peak current (Fig. 4f, Supplementary Fig. S8). The peak current increased linearly for strains from 0.06 to 0.1 and strain rates from 0 to 0.4 s^{-1}. As a result, we were able to enhance the current output up to a value of 6 nA. Furthermore, we demonstrated the possibility of combining a number of our devices to yield higher levels of current and voltage. When two devices of the same polarity and similar electromechanical response were combined in parallel or serial configurations, we observed increased output current or voltage signals, respectively (Fig. 4g,h). This indicates that our phage-based piezoelectric devices can be scaled up to generate a higher energy output. Finally, while applying mechanical pressure to the phage-piezoelectric devices, we could turn on a liquid-crystal display and visualize the power output of our device (Supplementary Movie S2; for detailed procedures see Supplementary Information). As such, we have confirmed that these viral particles effectively behave as piezoelectric nanofibres with the potential for powering microelectronic devices.

At present, the piezoelectricity of biomaterials is not fully understood at the molecular level[33]. Unlike inorganic piezoelectric materials, biomaterials commonly show discrepancies in relation to the behaviours predicted by classic piezoelectric theories. This mismatch is attributed to the heterogeneity and hierarchical structure of biomaterials, features that are not accounted for in classic models based on idealized, crystalline structures. For example, collagen matrices exhibit a complex piezoelectric behaviour that in some cases cannot be explained by classical theory[9,33]. Both phage and collagen fibrils exhibit shear piezoelectricity[9]. Moreover, smectically ordered phage and collagen are aligned along a preferred axis with hexagonal packing[9,23]. Based on previous symmetry considerations, the smectically ordered phage can be described as having either D_6 or C_6 symmetry[9,33].

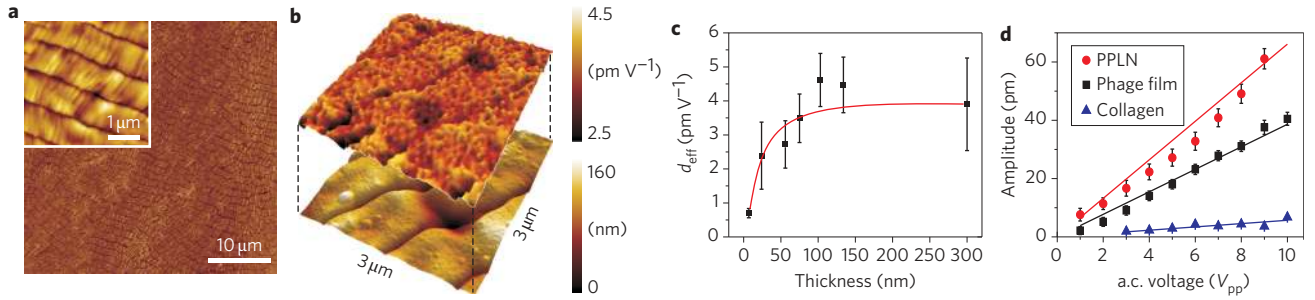

Figure 3 | Piezoelectric properties of multilayer 4E-phage films. a, AFM topography image of long-range ordered smectic phase liquid-crystalline film structure. Inset: AFM image showing smectic-aligned phage particles in ~1 μm bands. **b**, Effective piezoelectric coefficient d_{eff} mapping image (top) and AFM topography image (bottom) of smectic phase ordered phage films. **c**, Dependence of piezoelectric response of 4E-phage films on film thickness. **d**, Comparison of piezoresponse of phage films with those of PPLN and collagen films. Error bars in **c** and **d** indicate one standard deviation.

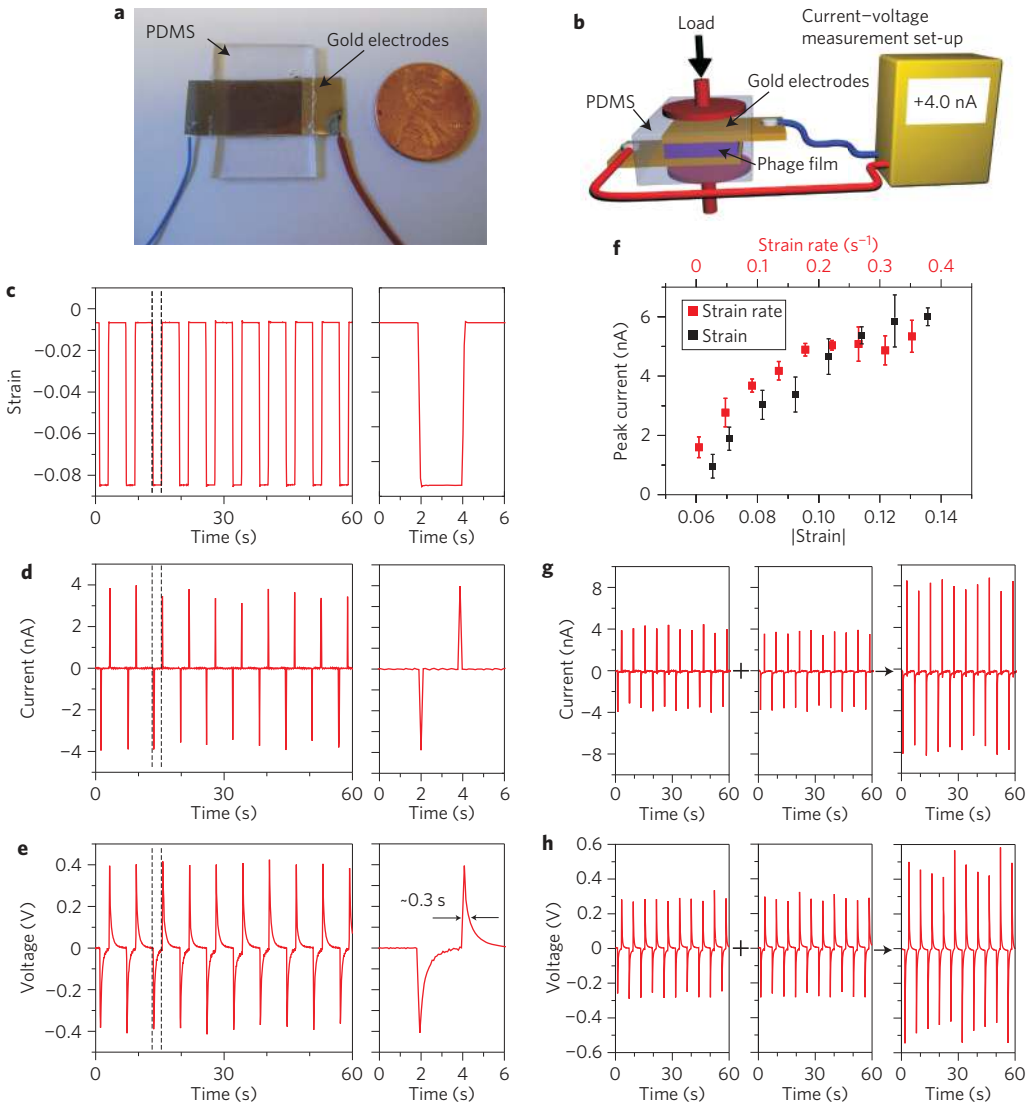

Figure 4 | Characterization of phage-based piezoelectric energy generator. a, Photograph of a phage-based generator. **b**, Schematic of piezoelectric electrical energy generation measurement set-up. A mechanical load was applied to the device while monitoring the voltage and current. **c**, Mechanical strain applied onto the device. **d**,**e**, Short-circuit current signal (**d**) and open-circuit voltage signal (**e**) from the phage-based generator. The two vertical dotted lines indicate the application (left line) and release (right line) of the load; a zoomed-in region is reported on the right. **f**, Dependence of phage-based generator peak current amplitude on strain and strain rate. Strain is defined as the ratio of device vertical displacement to initial device thickness, strain rate is defined as the strain change rate per unit time. **g**,**h**, Short-circuit current (**g**) and open-circuit voltage (**h**) summation of two different devices, under simultaneous mechanical stimulus. The signals from the two devices (left and middle panels) add to give increased current and voltage signals (right panels) when the devices are connected in parallel (**g**) and serial (**h**) connections (Supplementary Movie S2).

However, the piezoelectric coefficients corresponding to crystals with such symmetry do not fully explain the origin of the piezoelectricity we observed from our films although in the case of collagen matrices, the discrepancies could be partially reconciled by the use of space-dependent piezoelectric matrices and stress and stress-gradient induced polarization[33]. Therefore, we currently postulate that similar mechanisms are at play for our films, but additional mechanistic details will require further investigation.

In summary, we have developed a biopiezoelectric device made of genetically modified bacterial viruses (M13 phages). The liquid-crystalline property of these phages enables self-assembly into phage films, resulting in the simple fabrication of piezoelectric generators with sufficient energy output to turn on a liquid-crystal display. A higher energy output can be obtained by combining ordered phage films[23] in series or parallel configurations. Our phage-based materials exhibit the reverse piezoelectric effect—as demonstrated by PFM measurements—suggesting possible uses as actuators and energy harvesters, especially for integration into miniature-scale devices. Additional levels of control and optimization may come from exploring different viral particles and their diverse structural proteins, as long as they have suitably aligned dipoles[11,23].

Methods

Genetic engineering of phage. We constructed engineered phages using recombinant DNA engineering methods. Different numbers of glutamates were expressed at the N-terminus of the M13 major coat protein, positioned between the first and fifth amino acids of wild-type pVIII, replacing residues 2–4. The constructed phages were amplified using *Escherichia coli* cultures, purified using polyethylene glycol precipitation, and filtered through membranes with 0.45 μm pores. To verify phage stability, DNA sequences were confirmed at each step of the amplification.

Fabrication of piezoelectric phage films. To fabricate monolayer phage films, a polydimethylsiloxane (PDMS) stamp with a striped pattern was used to generate 2-μm-wide lines in an octadecanethiol self-assembled monolayer with 1 μm interline spacing on a gold-coated silicon substrate. A monolayer of phage was coated onto the cysteamine pattern using a phage-coating method as previously reported[31]. The octadecanethiol (ODT)/cysteamine patterned substrate (with a vertical cysteamine stripe pattern) was vertically dipped into a phage solution and pulled out at a constant speed (1.2 cm h^{-1}) using a home-built pulling machine controlled by a computer-programmed system. To fabricate multilayer phage films, either the pulling method or the dropcast method was used. With the pulling method, we obtained multilayer phage films with a thickness of up to ~300 nm. To obtain liquid-crystalline phage films with thicknesses greater than 300 nm, we used the dropcast method, in which 100 μl of phage solution (2 mg ml^{-1} in deionized water) was dropped onto a gold substrate and kept in a desiccator for three days.

Piezoelectric response characterization. To characterize monolayer phage films, we used an AFM set-up (Multimode, Veeco) with a Nanoscope IV controller under ambient conditions. The effective piezoelectric coefficient d_{eff} of monolayer phages was measured using an MFP-3D atomic force microscope (Asylum Research) with a platinum-coated AC240TS (Olympus) tip with a nominal spring constant of ~2 nN nm^{-1}, free-air resonance frequency of ~70 kHz and tip radius of ~7 nm, according to manufacturers' specifications.

Fabrication of phage-based piezoelectric generators. Gold-coated flexible substrates were prepared by depositing 10 nm chromium and 30 nm gold on Thermanox (Ted Pella) films. Then, 200 μl of 5 mg ml^{-1} 4E-phage solution was dropped on the gold-coated flexible substrate. After completely drying, another gold-coated flexible substrate was overlaid on the film. The device was then embedded between two ~2.5-mm-thick PDMS matrices to achieve structural stability. Signal wires were then soldered onto the gold electrodes.

Piezoelectric generator characterization. The phage-piezoelectric device was mounted onto a dynamic mechanical test system (Electroforce 3200, Bose), and a predefined displacement was applied while monitoring the total force on the device with a load cell. The actual displacement was monitored by a linear variable differential transformer installed in the Electroforce 3200. The force values from the load cell were multiplied by the ratio of the phage film area to the total device area to obtain the effective load applied to the phage film. The open-circuit voltages and short-circuit currents were measured using a semiconductor parameter analyser (4200-SCS, Keithley). Full methodological details can be found in the Supplementary Information.

Received 27 February 2012; accepted 12 April 2012; published online 13 May 2012

References

1. Damjanovic, D. Ferroelectric, dielectric and piezoelectric properties of ferroelectric thin films and ceramics. *Rep. Prog. Phys.* **61,** 1267–1324 (1998).
2. Galhardi, M. A., Guilherme, T. H. & Junior, V. L. A review of power harvesting on mechanical vibration using piezoelectric materials and applications, in *Proc. 7th Brazilian Conference on Dynamics, Control and Applications* 1005–1013 (Universidade Estadual Paulista (UNESP), 2008).
3. Chen, X., Xu, S. Y., Yao, N. & Shi, Y. 1.6 V nanogenerator for mechanical energy harvesting using PZT nanofibers. *Nano Lett.* **10,** 2133–2137 (2010).
4. Hu, Y., Lin, L., Zhang, Y. & Wang, Z. L. Replacing a battery by a nanogenerator with 20 V output. *Adv. Mater.* **24,** 110–114 (2012).
5. Wang, Z. L. & Song, J. Piezoelectric nanogenerators based on zinc oxide nanowire arrays. *Science* **312,** 242–246 (2006).
6. Chang, C., Tran, V. H., Wang, J., Fuh, Y-K. & Lin, L. Direct-write piezoelectric polymeric nanogenerator with high energy conversion efficiency. *Nano Lett.* **10,** 726–731 (2010).
7. Saito, Y. *et al.* Lead-free piezoceramics. *Nature* **432,** 84–87 (2004).
8. Bassett, C. A. L. & Becker, R. O. Generation of electric potentials by bone in response to mechanical stress. *Science* **137,** 1063–1064 (1962).
9. Fukada, E. Piezoelectric properties of biological polymers. *Q. Rev. Biophys.* **16,** 59–87 (1983).
10. Minary-Jolandan, M. & Yu, M-F. Nanomechanical heterogeneity in the gap and overlap regions of type I collagen fibrils with implications for bone heterogeneity. *Biomacromolecules* **10,** 2565–2570 (2009).
11. Farrar, D. *et al.* Permanent polarity and piezoelectricity of electrospun α-helical poly(α-amino acid) fibers. *Adv. Mater.* **23,** 3954–3958 (2011).
12. Kholkin, A., Amdursky, N., Bdikin, I., Gazit, E. & Rosenman, G. Strong piezoelectricity in bioinspired peptide nanotubes. *ACS Nano* **4,** 610–614 (2010).
13. Lee, S-W., Mao, C., Flynn, C. E. & Belcher, A. M. Ordering of quantum dots using genetically engineered viruses. *Science* **296,** 892–895 (2002).
14. Douglas, T. & Young, M. Host–guest encapsulation of materials by assembled virus protein cages. *Nature* **393,** 152–155 (1998).
15. Naik, R. R., Stringer, S. J., Agarwal, G., Jones, S. E. & Stone, M. O. Biomimetic synthesis and patterning of silver nanoparticles. *Nature Mater.* **1,** 169–172 (2002).
16. Lee, Y. J. *et al.* Fabricating genetically engineered high-power lithium-ion batteries using multiple virus genes. *Science* **324,** 1051–1055 (2009).
17. Nam, Y. S. *et al.* Biologically templated photocatalytic nanostructures for sustained light-driven water oxidation. *Nature Nanotech.* **5,** 340–344 (2010).
18. Merzlyak, A., Indrakanti, S. & Lee, S. W. Genetically engineered nanofiber-like viruses for tissue regenerating materials. *Nano Lett.* **9,** 846–852 (2009).
19. Rong, J. *et al.* Oriented cell growth on self-assembled bacteriophage M13 thin films. *Chem. Commun.* 5185–5187 (2008).
20. Smith, G. P. & Petrenko, V. A. Phage display. *Chem. Rev.* **97,** 391–410 (1997).
21. Dogic, Z. & Fraden, S. Smectic phase in a colloidal suspension of semiflexible virus particles. *Phys. Rev. Lett.* **78,** 2417–2420 (1997).
22. Kalinin, S. V. & Bonnell, D. A. Imaging mechanism of piezoresponse force microscopy of ferroelectric surfaces. *Phys. Rev. B* **65,** 125408 (2002).
23. Chung, W-J. *et al.* Biomimetic self-templating supramolecular structures. *Nature* **478,** 364–368 (2011).
24. Bhattacharjee, S., Glucksman, M. J. & Makowski, L. Structural polymorphism correlated to surface charge in filamentous bacteriophages. *Biophys. J.* **61,** 725–735 (1992).
25. Marvin, D. A., Welsh, L. C., Symmons, M. F., Scott, W. R. P. & Straus, S. K. Molecular structure of fd (f1, M13) filamentous bacteriophage refined with respect to X-ray fibre diffraction and solid-state NMR data supports specific models of phage assembly at the bacterial membrane. *J. Mol. Biol.* **355,** 294–309 (2006).
26. Yoo, S. Y., Chung, W-J., Kim, T. H., Le, M. & Lee, S-W. Facile patterning of genetically engineered M13 bacteriophage for directional growth of human fibroblast cells. *Soft Matter* **7,** 363–368 (2011).
27. Kim, D. M. *et al.* Thickness dependence of structural and piezoelectric properties of epitaxial $Pb(Zr_{0.52}Ti_{0.48})O_3$ films on Si and $SrTiO_3$ substrates. *Appl. Phys. Lett.* **88,** 142904 (2006).
28. Durkan, C., Welland, M. E., Chu, D. P. & Migliorato, P. Probing domains at the nanometer scale in piezoelectric thin films. *Phys. Rev. B* **60,** 16198–16204 (1999).
29. Jungk, T., Hoffmann, A. & Soergel, E. Contrast mechanisms for the detection of ferroelectric domains with scanning force microscopy. *New J. Phys.* **11,** 033029 (2009).
30. Minary-Jolandan, M. & Yu, M. F. Nanoscale characterization of isolated individual type I collagen fibrils: polarization and piezoelectricity. *Nanotechnology* **20,** 085706 (2009).

31. Newman, B. A., Kim, K. G. & Scheinbeim, J. I. Effect of water content on the piezoelectric properties of nylon 11 and nylon 7. *J. Mater. Sci.* **25,** 1779–1783 (1990).
32. Wan, Y., Xie, L., Zhang, X. & Zhong, Z. Time dependence of piezoelectric d_{33} coefficient of cellular ferroelectret polypropylene film. *Appl. Phys. Lett.* **98,** 122902 (2011).
33. Elmessiery, M. A. Physical basis for piezoelectricity of bone-matrix. *IEE Proc. A* **128,** 336–346 (1981).

Acknowledgements

The authors thank Jiyoung Chang and Liwei Lin (University of California, Berkeley) for help with device fabrication and signal measurement. This work was supported by the National Science Foundation Center of Integrated Nanomechanical Systems (EEC-0832819) and the Laboratory Directed Research and Development fund from the Lawrence Berkeley National Laboratory.

Author contributions

B.Y.L. and S.W.L. conceived the experiment. B.Y.L., J.Z., C.Z. and J.M. performed PFM experiments. W.C., J.M. and C.Z. prepared the phage monolayer and multilayer films. Y.S.Y. prepared the genetically engineered phages. B.Y.L. fabricated the energy-generating devices and carried out measurement of the signals. B.Y.L. and E.W. performed the nanoindentation experiments on phage films. E.W. modelled the electrostatic potential of phage coat proteins. B.Y.L., J.Z., J.M., R.R. and S.W.L. analysed the data. B.Y.L., C.Z., E.W. and S.W.L. wrote the manuscript.

Additional information

The authors declare no competing financial interests. Supplementary information accompanies this paper at www.nature.com/naturenanotechnology. Reprints and permission information is available online at http://www.nature.com/reprints. Correspondence and requests for materials should be addressed to S.W.L.